



HAL
open science

Dynamics and energy dissipation of collisional blast waves in a perpendicular magnetic field

A. Triantafyllidis, J.-R. Marquès, Y. Benkadoum, Y. de León, A. Ciardi, J. Béard, Jean-Marc Lagarrigue, N. Ozaki, M. Koenig, A. Dearling, et al.

► **To cite this version:**

A. Triantafyllidis, J.-R. Marquès, Y. Benkadoum, Y. de León, A. Ciardi, et al.. Dynamics and energy dissipation of collisional blast waves in a perpendicular magnetic field. *Physics of Plasmas*, 2025, 32 (2), 10.1063/5.0238064 . hal-04957357

HAL Id: hal-04957357

<https://hal.science/hal-04957357v1>

Submitted on 19 Feb 2025

HAL is a multi-disciplinary open access archive for the deposit and dissemination of scientific research documents, whether they are published or not. The documents may come from teaching and research institutions in France or abroad, or from public or private research centers.









L'archive ouverte pluridisciplinaire **HAL**, est destinée au dépôt et à la diffusion de documents scientifiques de niveau recherche, publiés ou non, émanant des établissements d'enseignement et de recherche français ou étrangers, des laboratoires publics ou privés.



Distributed under a Creative Commons Attribution 4.0 International License

RESEARCH ARTICLE | FEBRUARY 06 2025

Dynamics and energy dissipation of collisional blast waves in a perpendicular magnetic field

A. Triantafyllidis ; J.-R. Marquès ; Y. Benkadoum; Y. De León ; A. Ciardi ; J. Béard ; J.-M. Lagarrigue; A. Dearling ; N. Ozaki ; M. Koenig ; B. Albertazzi



Phys. Plasmas 32, 022102 (2025)

<https://doi.org/10.1063/5.0238064>



View
Online



Export
Citation



Physics of Plasmas

Special Topics Open
for Submissions

[Learn More](#)

Dynamics and energy dissipation of collisional blast waves in a perpendicular magnetic field

Cite as: Phys. Plasmas **32**, 022102 (2025); doi: 10.1063/5.0238064

Submitted: 9 September 2024 · Accepted: 19 January 2025 ·

Published Online: 6 February 2025



View Online



Export Citation



CrossMark

A. Triantafyllidis,^{1,a)} J.-R. Marquès,¹ Y. Benkadoum,¹ Y. De León,¹ A. Ciardi,² J. Béard,³ J.-M. Lagarrigue,³ A. Dearling,^{4,b)} N. Ozaki,^{5,6} M. Koenig,¹ and B. Albertazzi^{1,c)}

AFFILIATIONS

¹LULI - CNRS, CEA, Sorbonne Universités, École Polytechnique, Institut Polytechnique de Paris, F-91120 Palaiseau cedex, France

²Sorbonne Université, Observatoire Paris, Université PSL, CNRS, Laboratoire d'Étude de l'Univers et des Phénomènes Extrêmes, LUX, F-75005 Paris, France

³Laboratoire National des Champs Magnétiques Intenses, LNCMI-CNRS, EMFL, Université Grenoble-Alpes, Université Paul Sabatier, Institut National des Sciences Appliquées, F-31400 Toulouse, France

⁴York Plasma Institute, University of York, York YO10 5DD, United Kingdom

⁵Graduate School of Engineering, Osaka University, Suita, Osaka 565-0871, Japan

⁶Institute of Laser Engineering, Osaka University, Suita, Osaka 565-0871, Japan

^{a)} Author to whom correspondence should be addressed: angelos.triantafyllidis@polytechnique.edu

^{b)} Also at: Blackett Laboratory, Imperial College London, London SW7 2BZ, United Kingdom

^{c)} Electronic mail: bruno.albertazzi@polytechnique.edu

ABSTRACT

We experimentally investigate the evolution and dynamics of laser-produced collisional blast waves (BW) under the influence of a perpendicular magnetic field up to 20 T. We show that an external magnetic field causes the BW to diverge from the Taylor–Sedov solution while also impacting its structural morphology. We notably explore the significance of various magnetohydrodynamic (MHD) processes occurring on scales similar to the width of the BW front by comparing their characteristic lengths to it and demonstrate that the downstream plasma's transition from being super- to sub-magnetosonic plays a pivotal role in the overall structure. Our results show that multiple MHD effects can contribute to shaping a magnetized BW, illustrating the complexity of the underlying physics.

© 2025 Author(s). All article content, except where otherwise noted, is licensed under a Creative Commons Attribution (CC BY) license (<https://creativecommons.org/licenses/by/4.0/>). <https://doi.org/10.1063/5.0238064>

I. INTRODUCTION

Understanding the structure of blast waves (BW) under the influence of an external magnetic field is essential in numerous systems. In astrophysics, the interaction between the ever-present magnetic fields¹ and low-density, collisionless shocks can influence the structure of the interstellar medium (ISM)^{2–4} and the propagation of supernova remnants (SNR).^{5–7} Recent work in inertial confinement fusion (ICF) suggests that magnetic fields may contribute to achieving the necessary conditions for high fusion yields as well as introduce anisotropy in the shock structure.⁸ Additionally, several advancements have been made throughout the last few years aiming to characterize the dynamics of collisional shock waves generated by kilojoule nanosecond lasers in laboratory astrophysics experiments.^{9–14} The physics of (collisional) shocks is highly relevant to these active fields, and comprehending how a magnetic field affects the processes that participate in these phenomena is crucial.

Magnetohydrodynamics (MHD) predicts that multiple effects can impact the propagation of a BW under a large-scale magnetic field, drastically complicating the shock structure.^{15–19} While pure hydrodynamic shocks can be considered as consisting of two distinct areas (upstream and downstream) with an infinitely thin discontinuity separating them, the generation of entropy necessitates the existence of a finite transition region shock or BW front. More specifically, the thermodynamic quantities must transition from the unshocked to the shocked fluid's conditions via various dissipative and dispersive processes that exhibit structures with characteristic length scales. Experimentally measuring the length scales that arise in magnetized BWs helps to discriminate the dominant physical mechanisms in the system.

Among these, Ohmic heating has been found to play a major role in the morphology of MHD shocks.^{16,20} A separation of charges can occur on a scale equal to the ion inertial length $d_i = c/\omega_{pi}$, where ω_{pi}

is the ion plasma frequency, meaning that magnetization of electrons is possible while ions remain non-magnetized.^{21,22} In the resistive MHD regime, the subsequent generation of an electric potential acts on the electrons, forming an electron drift current perpendicular to the shock front that heats it ohmically and dissipates energy. This mechanism will satisfy the MHD shock jump conditions only if the magnetosonic Mach number $M_{ms} = v_s/v_{ms}$ is below a certain value, the critical Mach number $M_{ms,c}$ (subcritical shock), where v_{BW} is the BW velocity, $v_{ms} = \sqrt{v_A^2 + c_s^2}$ is the upstream ion-magnetosonic velocity, $v_A = \frac{B_0}{\sqrt{\mu_0 \rho_n}}$ is the Alfvén velocity upstream (ions and neutrals are considered to be strongly coupled²³), B_0 is the amplitude of the magnetic field, ρ_n is the mass density of the neutrals, and c_s is the sound velocity of the medium. Otherwise, if $M_{ms} > M_{ms,c}$, Ohmic heating is unable to achieve sufficient diffusion, and other processes are necessary to bridge the gap between the fluid upstream and downstream.

Other scale lengths that could be important include the ion inertial length and the one arising from viscous dissipation (Ion-ion mean free path, mfp), the gyration of ions and electrons due to the magnetic field (gyroradius), thermal diffusion, lower hybrid turbulence, and ambipolar diffusion. The latter one is relevant when v_{BW} is smaller than the ion-magnetosonic velocity v_{ms} (but still larger than v_{ms} , see more in Ref. 2) in weakly ionized, low-density astrophysical plasmas, where the ions and neutrals decouple because of the magnetic field.^{2,24–27} A relative velocity develops between the two species, and momentum is transferred via ion-neutral scattering, resulting in the emergence of continuous shocks (C-type shocks). Ambipolar diffusion is thought to be an important mechanism in astrophysical shocks^{2,24–27} and has been proposed as a possible explanation behind multiple astronomical observations.^{28–31} Moreover, whether the downstream plasma is sub- or supermagnetosonic is decisive since some of the aforementioned processes stop being relevant for $M_{ms} < 1$, in which case the dynamics of the magnetic field itself could play a key role. Simulations have been performed to study these phenomena;^{32,33} however, the widely different scales involved (μm to mm in laboratory experiments) present a formidable challenge, especially in three dimensions.

Evidently, an experimental investigation of magnetized BWs is needed to determine the main processes that shape the system. Distinguishing between mechanisms that produce similar scale lengths requires taking measurements under a wide range of conditions. Russell *et al.*^{34,35} performed such an investigation, and their results support that in resistive MHD the transition region’s length equals the resistive diffusion length, as predicted by theory.^{15,16} Still, their work was inconclusive as it showed that two-fluid effects could also have a non-negligible impact on the system. Furthermore, Mabey *et al.*³⁶ examined the effect of a 10 T external magnetic field on a Taylor–Sedov BW.^{37,38} This study revealed structural modifications, a departure from spherical symmetry and changes in the BW’s propagation velocity as a result of the external magnetic field, but no definitive evidence of ambipolar diffusion was observed.

In this paper, we report on the results of an experiment where a laser-produced, collisional ($\text{mfp} \ll \text{shock width}$) BW expands in air and is permeated by an external, uniform magnetic field up to 20 T oriented perpendicularly to the BW’s propagation. The impact of the magnetic field on the BW dynamics is explored, and it is shown that its morphology changes remarkably due to multiple MHD effects. In addition, the presence of strong magnetic fields allows us to distinguish under which conditions each process could be relevant, but also document how the BW transitions from

super- to sub-magnetosonic, effectively being reduced to simple propagating plasma. Finally, our data make possible the benchmarking of numerical codes that have never been tested in the parameter range presented here.

II. EXPERIMENTAL SETUP

The experiment was performed at the LULI2000 laser facility at LULI (École Polytechnique, France). One long pulse laser beam ($\tau \approx 1.5\text{ns}$), with energy $E_0 \approx 600\text{J}$ per pulse and intensity of $I_0 \approx 3 \cdot 10^{14}\text{W/cm}^2$ at the 2ω frequency ($\lambda_L = 526.5\text{nm}$), was focused to a $200\mu\text{m}$ flat-top focal spot using a hybrid phase plate onto a $500\mu\text{m}$ cylindrical graphite pin. The short time and spatial scale of the deposited energy generates a BW that propagates in an ambient medium (air at $2 \pm 0.2 \cdot 10^{17}\text{cm}^{-3}$, 300 K). The magnetic field was generated using a coil in a Helmholtz configuration, developed by LNCMI. It can deliver a spatially uniform and temporally constant magnetic field (approximately 1cm^3 on a μs scale), of up to 20 T.³⁹

The experimental setup and the diagnostics that characterized the BWs are shown in Fig. 1. Mach–Zehnder interferometry was used to retrieve the electron density (n_e)⁴⁰ using a collimated Nd:YAG laser pulse as a probe beam ($\lambda_b = 532\text{nm}$, $E_0 \approx 1\text{mJ}$, $R \sim 1.5\text{cm}$, $\tau \approx 7\text{ns}$). The 2D plasma self-emission was captured in the 580 – 850nm wavelength range and revealed the morphology, evolution, and dynamics of the system. Both the interferometry and the 2D self-emission diagnostic probed the plasma from 5 to 50 ns with a time step of 5 or 10 ns for all values of the magnetic field. Streaked optical pyrometry (SOP) provided time-resolved information on the propagation of the BW from its creation until $\sim 50\text{ns}$ for every shot.⁴¹

A time-resolved optical spectrometer probed a small volume ($150 \times 150 \times 50\mu\text{m}^3$) located 4 mm in front of the graphite pin target with an $f/5.74$ collecting lens and a magnification of 4.9. The spectra were collected on the visible range (425 – 675nm), and the resolution of the instrument was $\Delta\lambda \sim 2\text{nm}$. The collected data, coupled with PrismSPECT simulations of nitrogen lines,⁴² enabled us to retrieve the BW’s electron density, electron temperature (T_e), and average ionization (Z) by using a chi-square test to select the best fits. The lines in the range of 445 to 510 nm were chosen because they are particularly sensitive to changes of n_e and T_e (see Figs. 2 and 3, also Albertazzi *et al.*¹² for more details). While oxygen and carbon plasmas are also present,

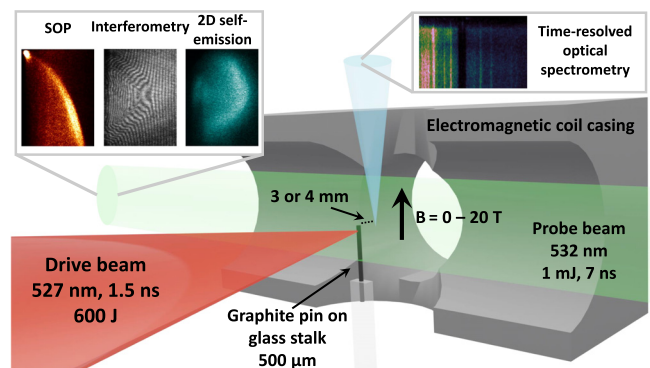


FIG. 1. Experimental setup at the LULI2000 facility. A laser beam was used to drive the target and generate a BW inside air. The SOP, interferometry, and 2D self-emission diagnostics collected the light coming from the transverse direction. A time-resolved optical spectrometer gathered the light originating 4 mm in front of the TCC.

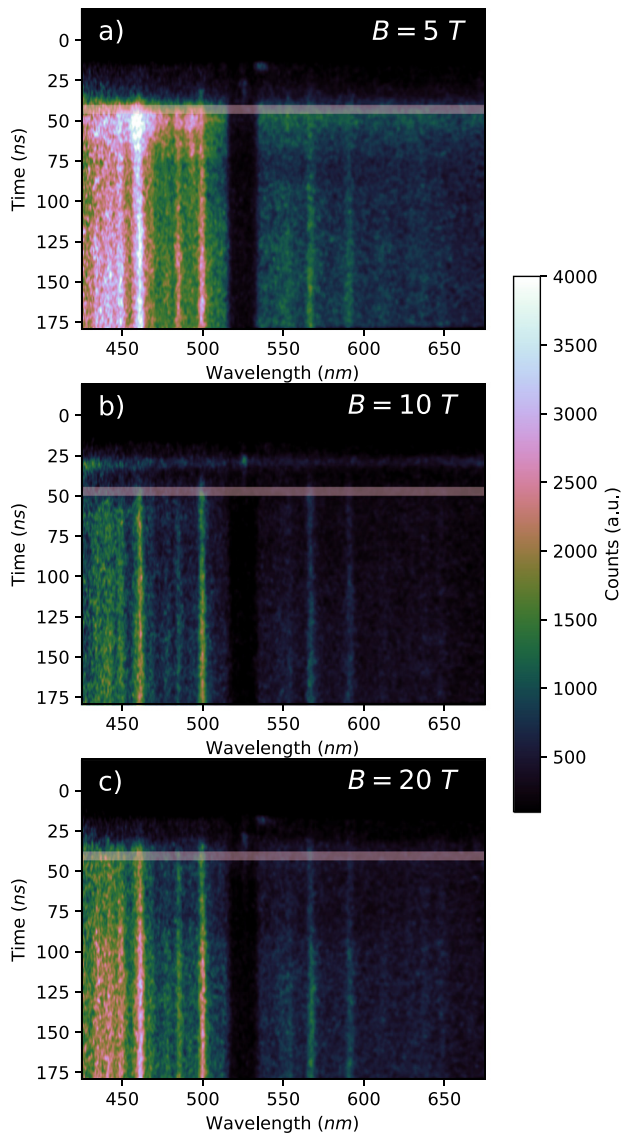


FIG. 2. Time-resolved spectra collected by the prism spectrometer in a small volume ($150 \times 150 \times 50 \mu\text{m}^3$) located 4 mm in front of the graphite pin target for a) 5 T , b) 10 T and c) 20 T . The shaded band indicates the time range over which the signal was time-integrated (see Fig. 3).

they have no intense lines in this specific range. The measured and derived quantities are presented in Table I.

III. RESULTS

A. Propagation of BWs in a magnetic field

The dynamic nature of MHD BWs requires a comprehensive understanding of the diverse forces at play. Here, four pressures are relevant: the ram, magnetic, thermal, and radiation pressures. Among them, the ram ($P_{\text{ram}} = \rho v_{\text{BW}}^2$) and the magnetic pressure ($P_{\text{mag}} = B^2/2\mu_0$) are the dominant ones by a large margin, with the ram pressure reaching approximately 1 kbar for a shock velocity of

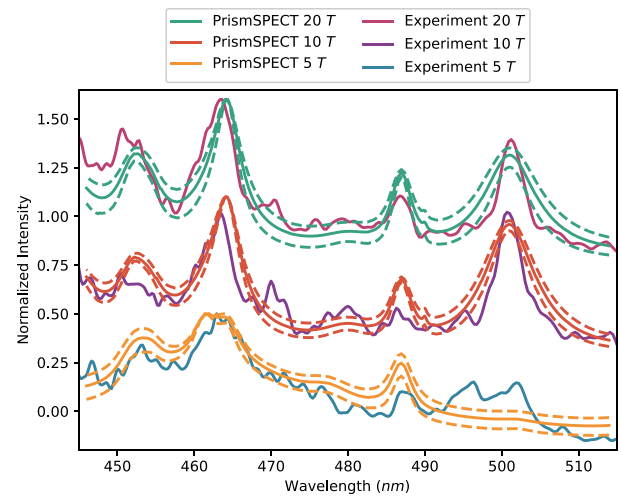


FIG. 3. Time-integrated lineouts (over 10 ns) for 5 , 10 , and 20 T . PrismSPECT simulations of constant T_e have been plotted over the experimental data. The best fits are plotted with solid lines, while dashed lines show the simulated spectra for $n_e \pm 1 \cdot 10^{18} \text{ cm}^{-3}$. Only nitrogen lines were considered.

around 100 km/s . In MHD, the magnetic Reynolds number $Re_m = vL/\eta$, where v is the plasma's velocity, L is the characteristic scale length of the system, and η is the plasma resistivity, gives an indication of the relative importance that advection and resistive diffusion play in the evolution of the magnetic field. At early times ($t \lesssim 5 \text{ ns}$), $Re_m \sim 10$, so resistive effects are relatively small, and the BW is able to push and compress the magnetic field, creating a diamagnetic cavity. However, at later times, as the BW decelerates, resistive effects across its front and throughout its radius become more important ($Re_m \gtrsim 1$); the compression of the magnetic field is then mediated by resistive diffusion, and it is relatively small. Since the BW decelerates significantly over time (e.g., $P_{\text{ram}}(t = 30 \text{ ns}) \approx 0.5 \text{ kbar}$), the dynamics will transition from being dominated by ram pressure ($\beta_{\text{dyn}} = P_{\text{ram}}/P_{\text{mag}} = M_{\text{ms}}^2 > 1$) to being magnetically dominated ($\beta_{\text{dyn}} = M_{\text{ms}}^2 < 1$). A lower estimate of the magnetic pressure is obtained by assuming that the magnetic field is uncompressed: 0.4 kbar for 10 T and 1.6 kbar for 20 T .

The interplay between the two dominant pressures is captured by the SOP diagnostic, as shown in Fig. 4 and Table II. At early times, regardless of the magnetic field amplitude, the BWs exhibit a similar behavior as P_{ram} largely dominates over P_{mag} ($\beta_{\text{dyn}} \gg 1$ and $c_s \ll v_A < v_{\text{BW}}$). The BWs exit their ballistic phase only after about 10 ns . Prior to this moment, and especially for low magnetic field values, they propagate with a very large velocity. The critical magnetosonic Mach number, which depends on $\beta_{\text{th}} = P_{\text{th}}/P_{\text{mag}}$ and on the shock angle, is $M_{\text{ms},c} \approx 2.9$ (for 90° and $c_s \ll v_A$, so $\beta_{\text{th}} \ll 1$)⁴³ and can be exceeded early on, making the shock supercritical: $M_{\text{ms}} \approx 13$ at 3 ns and $M_{\text{ms}} \approx 3$ at 10 ns for $B = 5 \text{ T}$.

Later on, in the absence of an external magnetic field, we expect the expansion of a BW to be described by the Taylor–Sedov solution ($R(t) = at^{b_{ST}}$, $b_{ST} = 0.4$). Indeed, using Fig. 4(a) and selecting multiple points of the BW front, we fit its trajectory and confirm that $b = b_{ST} = 0.4$. In contrast, with a strong applied magnetic field, a magnetic pressure gradient affects the dynamics of the BW to a large

TABLE I. The plasma parameters retrieved from the diagnostics (top) and the calculated quantities (bottom) of the front of the BW at 40 ns. The electron temperature T_e and density n_e were retrieved using time-resolved optical spectrometry 4 mm from TCC along the laser axis. The latter was also characterized using the interferometry diagnostic. Re_m was calculated using the radius of the BW as the characteristic scale length. Note that at 40 ns the plasma is no longer supermagnetosonic, but we keep the naming convention v_{BW} for consistency.

Parameter / Quantity	Symbol	0 T	5 T	10 T	15 T	20 T
BW velocity (km/s)	v_{BW}	35 ± 5	32.5 ± 7.5	20 ± 10	15 ± 5	10 ± 5
Electron number density (10^{18}cm^{-3})	n_e	6 ± 2	5 ± 2	3 ± 1	1.5 ± 0.3	1.2 ± 0.5
Electron temperature (eV)	T_e	16 ± 4	8.6 ± 1.5	5.5 ± 0.5	5.1 ± 0.2	5.1 ± 0.3
Average ionization	Z	4.9 ± 0.2	3.1 ± 0.2	2.4 ± 0.3	2.3 ± 0.2	2.3 ± 0.3
Alfven velocity (km/s)	v_A	0	47 ± 1	92 ± 2	141 ± 2	184 ± 6
Magnetosonic Mach number	M_{ms}	$\gg 1$	0.7	0.2	0.1	0.1
Dynamic beta	β_{dyn}	...	0.8	0.5	0.3	0.3
Magnetic Reynolds number	Re_M	...	3.0	1.5	1.1	0.8
Electron Hall parameter	$\omega_e \tau_e$	0	0.11 ± 0.05	0.27 ± 0.10	0.67 ± 0.20	1.10 ± 0.35

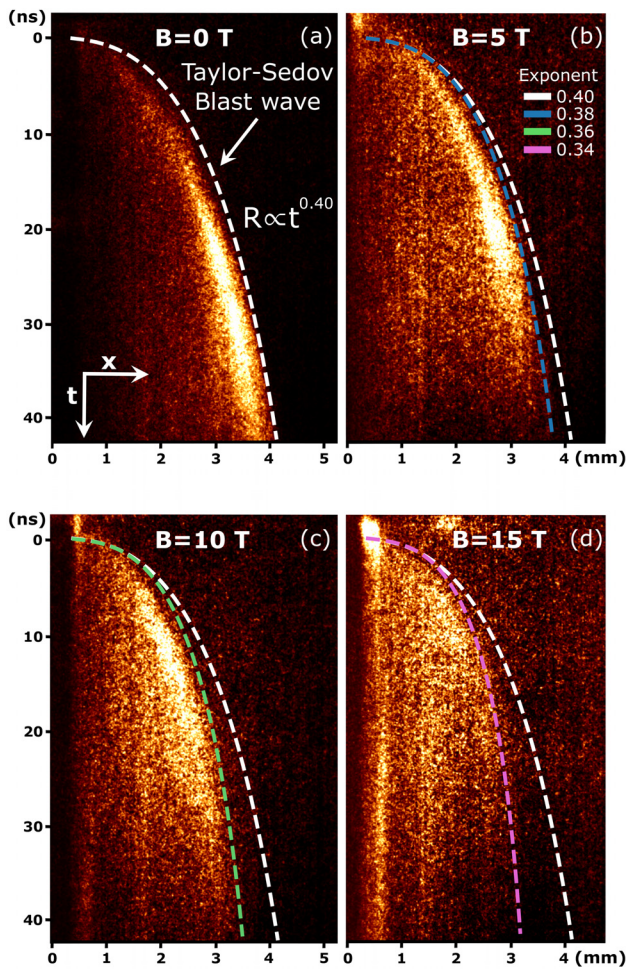


FIG. 4. Time-resolved self-emission (SOP) of the BW showing typical trajectories for (a) $B = 0 \text{ T}$ (Taylor-Sedov solution) (b) $B = 5 \text{ T}$ (c) $B = 10 \text{ T}$, and (d) $B = 15 \text{ T}$. The fit of the BW's trajectory becomes worse as the magnetic field strength increases, and it can no longer be described as $R(t) = at^b$. Note that for $t \leq 10 \text{ ns}$, the BW is still in its ballistic phase.

TABLE II. Approximate time ranges of the BW's evolution stages for every magnetic field value.

B (T)	Supercritical ($M_{ms} > 2.9$)	Subcritical ($1 \leq M_{ms} \leq 2.9$)	Sub-magnetosonic ($M_{ms} < 1$)
5	0–10 ns	10–37 ns	> 37 ns
10	0–7 ns	7–30 ns	> 30 ns
15	0–5 ns	5–15 ns	> 15 ns
20	0–3 ns	3–8 ns	> 8 ns

degree and the system is governed by P_{mag} ($c_s \ll v_{BW} < v_A$) or, in other words, the BW becomes sub-magnetosonic. Attempting the same treatment now fails, with the exponent b deviating more and more from b_{ST} as the magnetic field increases. More specifically, $b < 0.4$ in the presence of an external perpendicular magnetic field, meaning that the magnetic pressure gradient further decelerates the BW (see Fig. 5) and its propagation is no longer self-similar.

By approximating the BW as a black body, we get an upper estimate of the radiation pressure: $P_{rad,max} = (4\sigma/3c)T^4 \sim 15 - 300 \text{ mbar} \ll P_{ram} \sim P_{mag} \sim 1 \text{ kbar}$, for $T_e = 5 - 15 \text{ eV}$, respectively.

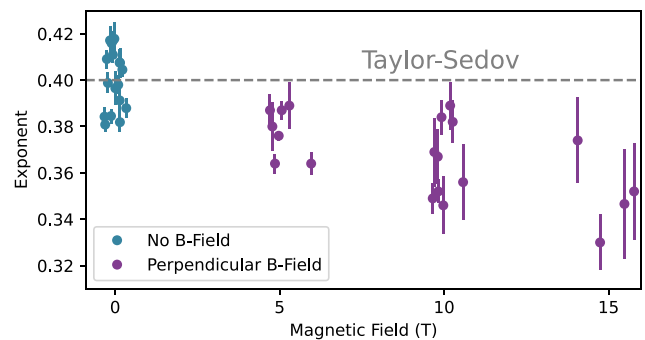


FIG. 5. Exponent b ($R(t) = at^b$) of the BW expansion as a function of the magnetic field amplitude. The error bars are given by the fitting algorithm and become larger as we increase the magnetic field strength due to the front's dissipation (see Fig. 6). The data points have been slightly displaced in the x-axis for better clarity.

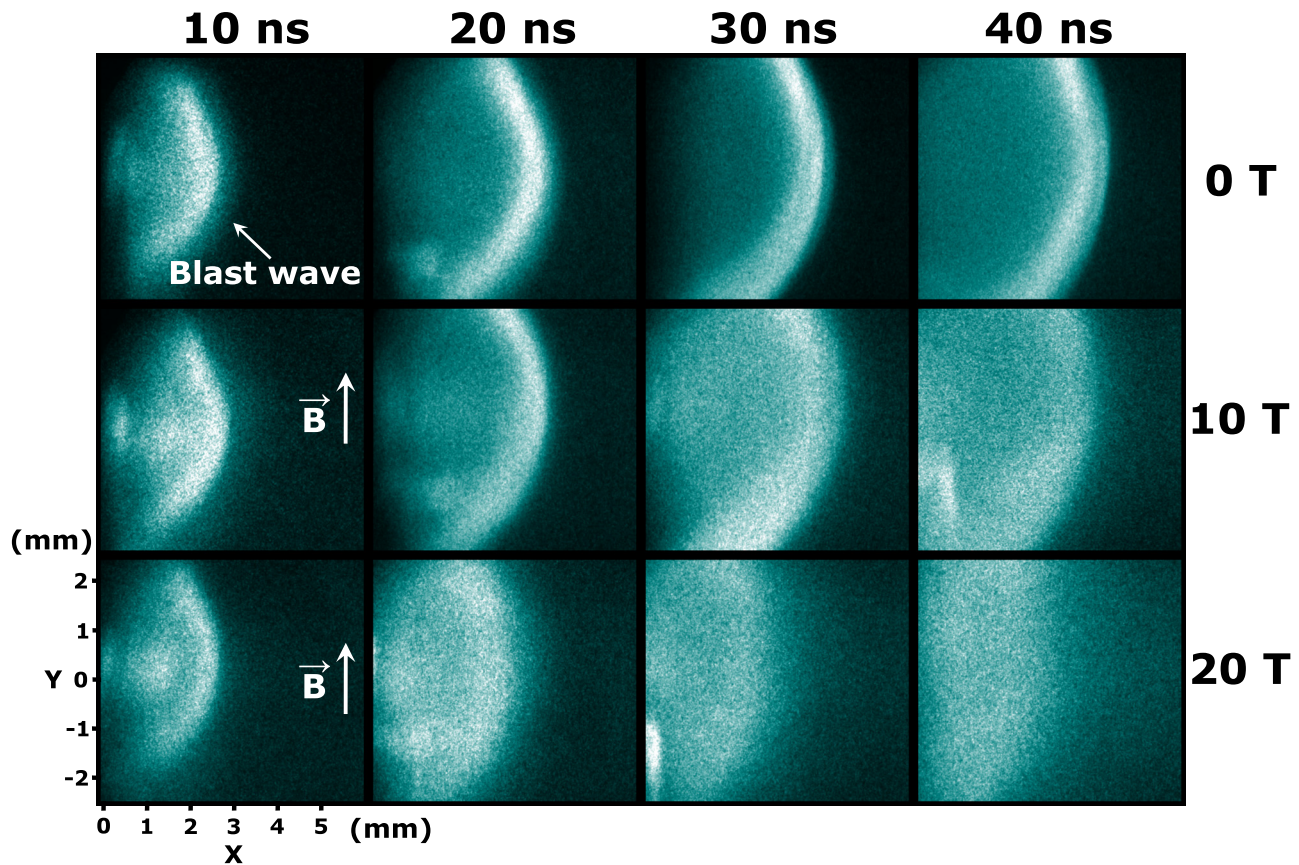


FIG. 6. 2D self-emission of the BW plasma in the 580 – 850nm wavelength range as a function of time and magnetic field amplitude. The graphite pin target is outside the field of view on the left of the images.

Therefore, the radiation pressure is negligible dynamically and does not participate in the evolution of the BWs, no matter the magnetic field strength. A more detailed discussion on radiative effects can be

found toward the end of the following subsection. The ambient thermal pressure P_{th} is also considered negligible, as it is also well below 1 bar.

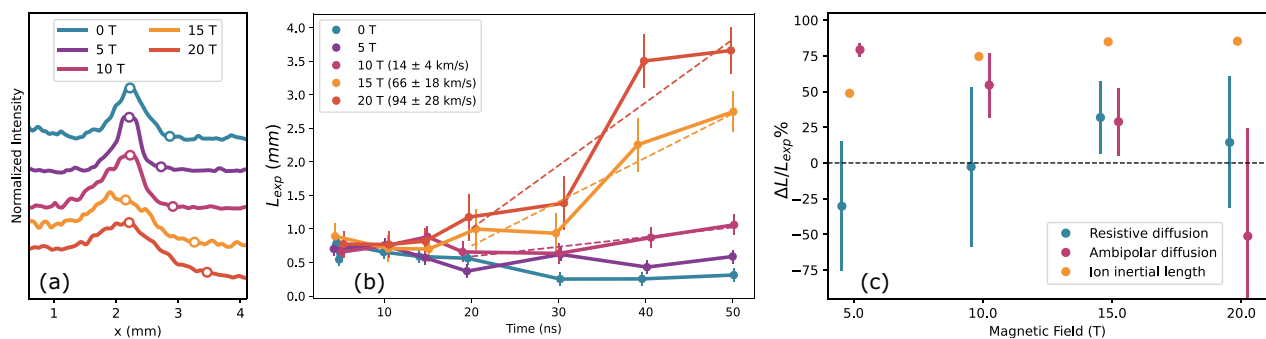


FIG. 7. (a) Lineouts of the 2D plasma self-emission images along the laser path ($y = 0$ in Fig. 6) for $B = 0 - 20T$ at $20 ns$, after applying an inverse Abel transform. The dots indicate approximately the distance L_{exp} that was measured. (b) The front width L_{exp} measured from the 2D plasma self-emission images between $5 - 50 ns$ and for $B = 0 - 20T$. The dashed lines indicate the slopes for the 10, 15 and 20 T cases. (c) Comparison between the front width and calculated scale lengths for all magnetic field values at $40 ns$. The y-axis shows the ratio of $\Delta L = L_{exp} - L$ over L_{exp} . The ion inertial length error bars are too small to be visible. Since the BW is sub-magnetosonic at $40 ns$ for most magnetic field values, ambipolar, and resistive diffusion cannot shape the BW width anymore. For ease of visualization, the data points in (b) and (c) have been slightly displaced in the time and magnetic field axes around their nominal value, respectively.

TABLE III. Calculations of the relevant scale lengths of the front of the BW at 40 ns. The electron and ion mean free path, as well as their gyroradii, are of the order of 10^{-2} mm or smaller for every case. Since the BW is sub-magnetosonic at 40 ns for most magnetic field values, ambipolar and resistive diffusion cannot shape the BW width anymore.

Length	Symbol	0 T	5 T	10 T	15 T	20 T
Measured BW front width (mm)	L_{exp}	0.26 ± 0.10	0.43 ± 0.10	1.28 ± 0.15	3.04 ± 0.35	3.50 ± 0.40
Ion inertial length (mm)	d_i	0.16 ± 0.01	0.22 ± 0.01	0.32 ± 0.02	0.46 ± 0.02	0.51 ± 0.03
Electron thermal diffusion length (10^{-2} mm)	L_χ	2.98 ± 2.12	1.42 ± 0.8	1.67 ± 0.70	3.50 ± 1.15	6.41 ± 2.32
Resistive diffusion length (mm)	L_η	...	0.56 ± 0.20	1.31 ± 0.70	2.07 ± 0.80	2.95 ± 1.59
Ambipolar diffusion length (mm)	L_{AD}	...	0.09 ± 0.02	0.58 ± 0.29	2.16 ± 0.72	5.30 ± 2.65

B. BW structure and energy dissipation

The 2D self-emission diagnostic reveals how the applied magnetic field shapes the BW's front. In the unmagnetized case (Fig. 6, top row), the pre- and post-shock regions are separated by a steep gradient in various macroscopic quantities, called the ion viscous shock (not directly resolvable here). According to Jaffrin & Probst (1964),²¹ it is embedded within two layers: first preceded by an upstream thermal heating layer, dominated by electron thermal conduction, and afterwards followed downstream by an equilibration layer, where electron and ion temperature reach equilibrium. The shock width, defined as the transition from this unperturbed state, is tens of times larger than the ion mean free path.

Under the influence of the perpendicular magnetic field, however (Fig. 6 middle and bottom rows), for values over 10 T and times longer than 20 ns, the BW front clearly starts to widen. The lineouts along the laser axis [see Fig. 7(a)] illustrate the gradual growth of the measured front width for increasing values of the magnetic field. Notably, Fig. 7(b) indicates that a transition takes place between 30 and 40 ns, leading to a sharp rise in the front width by a factor of 2 or more for $B \geq 15T$. As a consequence, the temperature of the now sub-magnetosonic plasma decreases substantially (see Table I) due to its energy spreading into a larger volume, and no clear boundary separating the downstream and upstream regions is observed. In addition, we observe the downstream plasma changing its shape from spherical to one with a broader edge, especially at 40 ns for 20 T when its front becomes noticeably flatter.

In order to distinguish the main energy dissipation mechanism and understand how the BW is shaped, we compare the characteristic scale length of the possible processes L with the measured magnetized BW's width L_{exp} . Then, we need to examine whether all conditions are met for these processes to affect the BW. L was measured using the 2D plasma self-emission diagnostic along the laser beam path ($y = 0$ in Fig. 6) between the background noise level and the point where the intensity plateaus, and it was plotted against time and magnetic field strength [Fig. 7(b)]. To avoid any artifacts, we averaged the intensity over a few pixels. Then, we calculated the quantity $\Delta L = L_{\text{exp}} - L$ and divided it by L_{exp} to compare the experimentally measured value with the theoretical one; positive values correspond to experimental lengths larger than what the theory predicts, while negative values indicate that the calculated length is larger than what was observed. Table III compares the measured and calculated scale lengths, and Fig. 7(c) graphically shows the comparison between the most relevant scale lengths (inertial ion length, resistive diffusion length, and ambipolar diffusion length).

The ion–ion, electron–electron, and electron–ion mean free paths are orders of magnitude smaller than the BW front's thickness (mf

$\leq 10^{-3}$ mm, assuming $T_e = T_i$). Consequently, the system is highly collisional, and viscous effects and the ion gyroradius do not shape the BW. Thermal conduction can also be ruled out as a dominant energy dissipation process, as the electron thermal diffusion length $L_\chi = \chi/v_{BW}$, where χ is the thermal conductivity given by Braginskii,⁴⁴ is negligible compared to L_{exp} ($10L_\chi \lesssim L_{\text{exp}}$). On the other hand, the ion inertial length, namely, the distance over which small-amplitude waves can disperse energy and make the shock less steep,^{18,22} is comparable to the BW's width for $B \leq 5T$, but considerably smaller for $B \geq 10T$. Thus, this mechanism could only contribute in the structure of the shock for relatively low magnetic fields and in the early moments of the BW propagation when it is supercritical (see Table II).

Ambipolar diffusion due to ion-neutral collisions allows disturbances to travel transversely to the magnetic field at the ion-magnetosonic velocity when $v_{BW} < v_{ims}$ (but $v_{BW} > v_{ms}$, full expressions found in Ref. 2), which reduces the jump between the downstream and upstream macroscopic quantities as the neutrals ahead of the BW front are heated. The discontinuity in the various thermodynamic quantities vanishes above a critical magnetic field value B_{crit} and the BW transitions to a continuous shock (C-shock). Using the MHD equations and assuming that the thermal and ram pressures of the ions are negligible, the ambipolar diffusion scale length is found to be²

$$L_{AD} \approx \frac{(m_i + m_n)B_0^2}{\pi\rho_i\rho_n\langle\sigma v\rangle_{in}v_{BW}} = \frac{m_i + m_n}{2\pi m_n\langle\sigma v\rangle_{in}} v_A^2 \cdot v_{BW}^{-1} \cdot n_n^{-1}, \quad (1)$$

where m_i , m_n are the ion and neutral masses, $\langle\sigma v\rangle_{in}$ is the rate coefficient of the ion-neutral scattering, and ρ_n , n_n are the mass and number densities of the neutrals, respectively (all expressed in cgs units).

The minimum value of the magnetic field for which an MHD shock wave can develop a magnetic precursor due to ambipolar diffusion is dependent on the ram and thermal pressures of the upstream gas,

$$B_{\text{min}}^2 = 4\pi[\rho_i v_{BW}^2 - \gamma n_e k_B (T_i + T_e)], \quad (2)$$

where γ is the adiabatic index and k_B is the Boltzmann constant.⁴⁵ From the generation of the BW to its dissipation, B_{min} is not constant. v_{BW} , n_e and T_e , as well as the ion temperature T_i change with time and they also depend on the strength of the initial magnetic field. Thus, for the conditions of this experiment, the minimum magnetic field value can vary from approximately 100 T early on to around 10 T at later times.

However, there is an issue concerning the significance of ambipolar diffusion in this regime. This process can only operate in weakly ionized plasmas because if the degree of ionization rises rapidly, v_{ims} will decrease and the shock will transition to one with a steep density gradient, much like in the unmagnetized case (J-type shock).^{3,46} The

outflow velocity exceeds the critical value over which molecules are rapidly dissociated for the majority of the BW's evolution,

$$\frac{m_n v_{crit}^2}{2} = I_{diss}, \quad (3)$$

where I_{diss} is the dissociation energy and $v_{crit} \approx 10\text{km/s}$ for molecular nitrogen.⁴⁷ Performing the same calculation for the first ionization energy of nitrogen results in $v_{crit} \approx 30\text{km/s}$. Importantly, the inequality $v_{ims} > v_{BW} > v_{ms} \approx v_A$ must hold, but v_A is significantly higher than v_{crit} when $B \neq 0\text{T}$. Therefore, ambipolar diffusion cannot contribute in shaping the BW in these experimental conditions, and its role is generally limited in laboratory experiments.

Finally, we can calculate the resistive diffusion length L_η by applying the appropriate resistivity model. It equals²⁰

$$L_\eta = \frac{\eta_\perp}{\mu_0 v_{BW}}, \quad (4)$$

where $\eta_\perp = 1.5 \cdot 10^7 Z/T_e (eV)^{3/2} [\text{cm}^2/\text{s}]$ is the resistivity perpendicular to the magnetic field⁴⁴ and μ_0 is the magnetic permeability of the vacuum. The electron Hall parameter $\omega_g \tau_e = e|B|\tau_e/m_e$ (see Table I), where ω_g is the gyrofrequency and τ_e is the electron-ion Coulomb collision time, quantifies the impact of gyromotion versus that of Coulomb collisions and demonstrates that, in our system, the aforementioned resistivity is valid for $B = 0, 5, 10$ and 15T ($\omega_g \tau_e < 1$).⁴⁸ However, $\omega_g \tau_e \sim 1$ for 20T , necessitating the use of the extended MHD (XMHD) model and the calculation of the full transport coefficients. Resistive diffusion's characteristic length shows the best agreement across all magnetic field values.

Still, one must be cautious in attributing the broadening of the BW front to resistive diffusion at the late stages and strong magnetic field cases, despite the good agreement between the measured and calculated values (see Table III). It is clear that in the 15 and 20T cases, v_{ms} becomes larger than the downstream plasma velocity v_{BW} very early in the BWs' propagation ($Re_m < 1$, see Tables I and II). This excludes the possibility that this diffusive process is responsible for the large increase in the front's length observed at $30 - 40\text{ns}$ and $B \geq 15\text{T}$ because $Re_m > 1$ is required. Instead, we need to consider the dynamics of the magnetic field itself as a possible explanation.

In the early stages of the phenomenon ($Re_m \sim 10$), the magnetic field is compressed by the plasma (indicated by its deceleration as a function of the magnetic field, see Figs. 4 and 5). This nonlinear perturbation of the magnetic field continues to travel along the propagation axis of the BW at the ion-magnetosonic velocity v_{ims} , independently of the now slower downstream plasma, possibly dragging along a part of it. This lasts until the magnetic field fully decompresses, a timescale approximated by the magnetic diffusion time

$$\tau_D \sim \frac{4\pi L^2}{\eta_\perp c^2}. \quad (5)$$

About $15 - 100\text{ns}$ are needed for the magnetic field to fully diffuse inside the front plasma, depending on the length scale used and the T_e of the plasma.

This is further supported by using Fig. 7(b) to calculate the slope of each set of points. This slope corresponds to the *relative velocity between the expanding BW front and the downstream plasma*. If we add to it the downstream plasma velocity, we find that the front plasma expands much faster than even the unmagnetized BW: $v_F(B = 15\text{T}, \Delta t = 20 - 40\text{ns}) \sim 85\text{km/s}$ and $v_F(B = 20\text{T}, \Delta t = 20 - 40\text{ns}) \sim 115\text{km/s}$. While these velocities do not equal $v_A (\approx v_{ims})$ for the

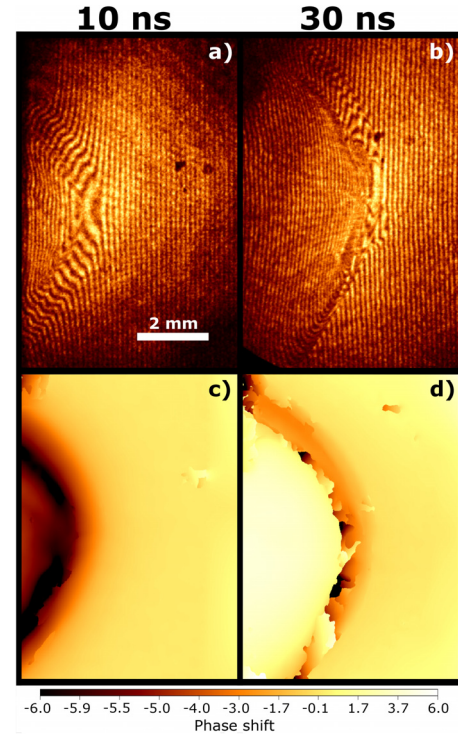


FIG. 8. (top) Interferograms for $B = 0\text{T}$ at a) 10 and b) 30ns . (bottom) Phase maps for the same shots at c) 10 and d) 30ns . The absence of a radiative precursor can be inferred due to the lack of a fringe shift ahead of the BW front.

respective magnetic field strengths, they are many times higher than the velocity of the BW at these times, strongly suggesting that the magnetic field is advecting part of the plasma. The discrepancy can be attributed to Re_m being near unity during these time frames. In this regime, no strong coupling exists between the plasma and the magnetic field, meaning that the plasma will not follow the magnetic field dynamics closely, although it can still be affected by it. Interestingly, for the $30 - 40\text{ns}$ time range, we calculate $v_F(B = 15\text{T}) \sim 130\text{km/s}$ and $v_F(B = 20\text{T}) \sim 210\text{km/s}$, when the respective Alfvén velocities are 141km/s and 184km/s .

Another process that is known to affect the structure of BWs is radiative losses. The existence of precursors due to radiative effects has been demonstrated in numerous experimental works,^{49–52} but we can distinguish between ones that can change the dynamics of the BWs (strong precursors) and the ones that cannot (weak precursors) using multiple methods. First, the expansion of a (strongly) radiative BW differs from that of a Taylor–Sedov BW in that it follows a trajectory $R(t) = at^b$ with $b < b_{ST} = 0.4$. That is to say that the BW will decelerate more as a result of radiative losses. Second, these intense radiative losses will ionize the ambient medium ahead of the BW front, creating a strong radiative precursor appearing as an electron density gradient with typically $T_e \sim 20 - 30\text{eV}$.^{50,53} In this case, interferometry or spectroscopy diagnostics can be used to resolve this feature. Crucially, strong radiative precursors have only been observed in BWs that propagate with $v_{BW} \geq 100\text{km/s}$ in a high Z gas such as xenon, and not in other gases commonly used in experiments (hydrogen, helium, nitrogen, argon, etc.).⁵¹

Nevertheless, some ionizing radiation is present in the majority of experiments where a strong laser pulse interacts with a solid target. Its

source could be the x-ray emission from the laser–target interaction or it could be caused by the high temperature of the plasma and post-shock region. However, this radiation can only produce weak precursors that are relatively cool and ionize the ambient medium mildly (see Albertazzi *et al.*¹²). More importantly, they have no effect on the dynamics of the BW, as the radiative losses are negligible, and they create barely resolvable structures ahead of the BW front.

The BWs presented in this paper fall into the second category: a small, cool radiative precursor can be inferred using the time-resolved optical spectrometry data, but not the interferometry data (see Fig. 8). Using PrismSPECT, an electron temperature of $T_e \sim 2eV$ and an average ionization of $Z \sim 0.8$ can be evaluated by fitting optical lines emission.¹² Furthermore, no dynamically important precursor exists in the most extreme case of $B = 0T$ (where we observed the highest v_{BW} and T_e , as well as a Taylor–Sedov expansion), making the emergence of a radiative precursor in the magnetized cases unlikely and placing significant constraints on how relevant this radiation can be.

Lower hybrid turbulence has also been thought to be connected to the heating of electrons and give rise to interesting features in magnetized plasmas,⁵⁴ but it seems that it cannot explain the observations here for a number of reasons. The threshold condition for this process is $L_n < r_{Li}(kv_i/\nu_e)^{1/2}$, where r_{Li} is the ion Larmor radius, $k = 2\pi/\lambda$ is the wavenumber, v_i is the ion thermal velocity, and ν_e is the collision frequency for e-e, e-i, and e-n collisions.⁵⁵ Substituting all the above parameters yields a scale length much too small to be observed ($L_n \sim 10^{-5}cm$). Additionally, lower hybrid turbulence is strongly inhibited by collisions; hence, we do not expect it to be relevant in this collisional system. Moreover, it cannot emerge because it simultaneously requires strongly magnetized electrons and unmagnetized ions.⁵⁵ However, the electron Hall parameter for $B = 20T$ is $\omega_g\tau_e \sim 1$ (see Table I), meaning that the effect of collisions is only approximately equal to that of gyration.

To summarize, we find that thermal diffusion, viscous effects, ambipolar diffusion, radiative losses, and lower hybrid turbulence can be ruled out as important processes in the studied regime. While the BWs are supermagnetosonic, the energy diffusion mechanism is resistive MHD effects (Ohmic heating). However, after the BWs transition to having $M_{ms} < 1$, the rapid extension of the front plasma suggests that a different mechanism is at play. More specifically, the magnetic field (that was being compressed while $M_{ms} \geq 1$) relaxes at a time frame that approximates the magnetic diffusion time t_D and interacts with the plasma by advecting part of it forwards with a velocity comparable to v_A . Nonetheless, the exact mechanism is not yet clear and more experimental evidence is needed to form more concrete conclusions.

IV. DISCUSSION AND CONCLUSIONS

It is apparent that multiple mechanisms can participate throughout the evolution of magnetized BWs. Dispersive effects at the ion inertial length scale can be important in the earliest stages when BWs are supercritical and Ohmic heating becomes the dominant mechanism after M_{ms} drops below the critical magnetosonic number. In such cases, the largest scale length governs the overall structure, but a double structure (sub-shock), characterized by two distinct scale lengths, may emerge if there is a significant enough change in the macroscopic variables across the shock.

However, after the BW decelerates to below the magnetosonic velocity, these dissipation mechanisms no longer define the BW width and the dynamics of the magnetic field possibly dominate the features that arise.

While the mechanisms proposed provide a plausible explanation for the observed phenomena, more evidence is necessary to validate these interpretations. Future experimental campaigns should aim to improve diagnostic capabilities to verify the plasma and magnetic field dynamics more precisely, e.g., by using time-resolved optical spectrometry data to detect the Zeeman splitting of emission lines.⁵⁶ Furthermore, numerical simulations that can account for the complex physical and chemical processes at play need to be performed if we are to draw confident conclusions. Due to the range of spatial and temporal scales involved, in addition to the variety of physical processes, kinetic or (multi)fluid modeling of these experiments is a formidable task.^{57–59} In this context, the data presented in this work can serve as a guide for future simulations.

To conclude, we have studied experimentally the formation and evolution of collisional BWs subjected to an external, perpendicular magnetic field of up to $20T$. We showed that in the presence of an ambient perpendicular magnetic field, the BW does not follow the Taylor–Sedov solution but decelerates drastically due to the magnetic pressure gradients acting on the expanding plasma. This offers insight into the dynamics of magnetized BWs in astrophysical contexts, such as supernova remnants and molecular clouds, where similar interactions can shape the evolution of shock structures.⁷ In both spherical and cylindrical shocks, azimuthal magnetic fields have been found to act as a counter-pressure to slow down their propagation in a similar manner.^{60,61} Furthermore, we compared the thickness of the transition region in a magnetized shock with the characteristic scale lengths of multiple processes and placed significant restrictions on their role. While we identified Ohmic heating as the dominant dissipation mechanism while the BW is supermagnetosonic, we demonstrated that the intricate nature of the phenomenon likely necessitates a combination of different mechanisms at different stages of the BW's evolution and a consideration of the magnetic field dynamics. This complicates attempts at numerically simulating the BWs shown here, but our work can be used in several potentially valuable ways. Examples include the benchmarking of numerical codes for magnetized laboratory astrophysics experiments and magnetized ICF experiments where an extreme compression of the magnetic field could significantly affect the plasma dynamics, as well as the understanding of shock propagation in magnetized astrophysical environments.

ACKNOWLEDGMENTS

The authors would like to thank the anonymous Referees for their insightful feedback, which significantly clarified the major points of our work. Also, we are grateful to the team at LULI2000 for their work in obtaining the data presented here. This work was benefited from state aid managed by l'Agence Nationale de la Recherche under the Investissements d'Avenir programs bearing the references ANR-18-EURE-0014, ANR-10-LABX-0039-PALM, and ANR-22-CE30-0044. For the purpose of Open Access, the authors have applied a CC-BY public copyright license to any Author Accepted Manuscript (AAM) version arising from this submission. N.O. was supported by grants from Japan Society for the Promotion of Science (JSPS) KAKENHI (Grants No. 23K20038) and JSPS Core-to-Core program (Grant No. JPJSCCA20230003).

AUTHOR DECLARATIONS

Conflict of Interest

The authors have no conflicts to disclose.

Author Contributions

A. Triantafyllidis: Conceptualization (lead); Data curation (lead); Formal analysis (lead); Investigation (lead); Methodology (lead); Resources (lead); Software (lead); Validation (lead); Visualization (lead); Writing – original draft (lead); Writing – review & editing (lead). **J.-R. Marquès:** Conceptualization (equal); Data curation (equal); Formal analysis (equal); Investigation (equal); Methodology (equal); Project administration (equal); Resources (equal); Software (equal); Supervision (equal); Validation (equal); Visualization (equal); Writing – review & editing (equal). **Y. Benkadoum:** Data curation (supporting); Formal analysis (supporting); Investigation (supporting); Methodology (supporting); Project administration (supporting); Supervision (supporting); Writing – review & editing (supporting). **Y. De León:** Formal analysis (supporting); Investigation (supporting); Methodology (supporting); Writing – review & editing (supporting). **A. Ciardi:** Conceptualization (equal); Formal analysis (supporting); Investigation (supporting); Methodology (equal); Supervision (equal); Writing – review & editing (equal). **J. Beard:** Investigation (supporting); Methodology (supporting); Resources (equal); Validation (equal); Writing – review & editing (supporting). **J.-M. Lagarrigue:** Investigation (supporting); Methodology (supporting); Resources (equal); Validation (equal); Writing – review & editing (supporting). **A. Dearing:** Data curation (supporting); Investigation (supporting); Methodology (supporting); Writing – review & editing (supporting). **N. Ozaki:** Data curation (supporting); Investigation (supporting); Methodology (supporting); Writing – review & editing (supporting). **M. Koenig:** Conceptualization (lead); Data curation (equal); Formal analysis (supporting); Funding acquisition (lead); Investigation (equal); Methodology (equal); Project administration (equal); Resources (equal); Supervision (lead); Validation (equal); Visualization (equal); Writing – review & editing (equal). **B. Albertazzi:** Conceptualization (lead); Data curation (lead); Formal analysis (supporting); Funding acquisition (lead); Investigation (equal); Methodology (equal); Project administration (lead); Resources (equal); Supervision (lead); Validation (equal); Visualization (equal); Writing – review & editing (equal).

DATA AVAILABILITY

The data that support the findings of this study are available from the corresponding author upon reasonable request.

REFERENCES

- ¹J. Han, *Annu. Rev. Astron. Astrophys.* **55**, 111 (2017).
- ²B. T. Draine, *Astrophys. J.* **241**, 1021 (1980).
- ³B. T. Draine and C. F. McKee, *Annu. Rev. Astron. Astrophys.* **31**, 373 (1993).
- ⁴D. R. Flower and G. Pineau des Forêts, *Mon. Not. R. Astron. Soc.* **297**, 1182 (1998).
- ⁵P. Slane, A. Bykov, D. C. Ellison, G. Dubner, and D. Castro, *Space Sci. Rev.* **188**, 187 (2015).
- ⁶S. Orlando, F. Bocchino, F. Reale, G. Peres, and P. Pagano, *Astrophys. J.* **678**, 274 (2008).
- ⁷J. West, S. Safi-Harb, T. Jaffe, R. Kothes, T. Landecker, and T. Foster, *Astron. Astrophys.* **587**, A148 (2016).
- ⁸C. A. Walsh, S. O'Neill, J. Chittenden, A. J. Crilly, B. Appelbe, D. J. Strozzi, D. Ho, H. Sio, B. Pollock, L. Divol *et al.*, *Phys. Plasmas* **29**, 042701 (2022).
- ⁹B. Albertazzi, A. Ciardi, M. Nakatsutsumi, T. Vinci, J. Béard, R. Bonito, J. Billette, M. Borghesi, Z. Burkley, S. Chen *et al.*, *Science* **346**, 325 (2014).
- ¹⁰B. Albertazzi, P. Mabey, T. Michel, G. Rigon, J. Marquès, S. Pikuz, S. Ryazantsev, E. Falize, L. Van Box Som, J. Meinecke *et al.*, *Matter Radiat. Extremes* **7**, 036902 (2022).
- ¹¹P. Mabey, B. Albertazzi, E. Falize, T. Michel, G. Rigon, L. Van Box Som, A. Pelka, F.-E. Brack, F. Kroll, E. Filippov *et al.*, *Sci. Rep.* **9**, 8157 (2019).
- ¹²B. Albertazzi, P. Mabey, T. Michel, G. Rigon, J.-R. Marquès, S. Pikuz, S. Ryazantsev, E. Falize, L. Van Box Som, J. Meinecke *et al.*, *Phys. Plasmas* **27**, 022111 (2020).
- ¹³H. G. Rinderknecht, H.-S. Park, J. Ross, P. Amendt, D. Higginson, S. Wilks, D. Haberberger, J. Katz, D. Froula, N. Hoffman *et al.*, *Phys. Rev. Lett.* **120**, 095001 (2018).
- ¹⁴R. Hua, J. Kim, M. Sherlock, M. Bailly-Grandvaux, F. Beg, C. McGuffey, S. Wilks, H. Wen, A. Joglekar, W. Mori *et al.*, *Phys. Rev. Lett.* **123**, 215001 (2019).
- ¹⁵F. De Hoffmann and E. Teller, *Phys. Rev.* **80**, 692 (1950).
- ¹⁶W. Marshall, *Proc. Roy. Soc. London. Ser. A. Math. Phys. Sci.* **233**, 367 (1955).
- ¹⁷R. Polovin, *Sov. Phys. Usp.* **3**, 677 (1961).
- ¹⁸C. F. Kennel, *J. Geophys. Res. Space Phys.* **93**, 8545, <https://doi.org/10.1029/JA093iA08p08545> (1988).
- ¹⁹R. P. Drake, *High-Energy-Density Phys.: Found. Inertial Fusion Exp. Astrophys.* **127**, 525–566 (2018).
- ²⁰F. Coroniti, *J. Plasma Phys.* **4**, 265 (1970).
- ²¹M. Y. Jaffrin and R. F. Probst, *Phys. Fluids* **7**, 1658 (1964).
- ²²R. Treumann, *Astron. Astrophys. Rev.* **17**, 409 (2009).
- ²³M. Suzuki and J. Sakai, *Astrophys. J.* **465**, 393 (1996).
- ²⁴D. F. Chernoff, *Astrophys. J.* **312**, 143 (1987).
- ²⁵J.-P. Chieze, G. P. des Forets, and D. Flower, *Mon. Not. R. Astron. Soc.* **295**, 672 (1998).
- ²⁶P. Lesaffre, J.-P. Chieze, and S. Cabrit, *Astron. Astrophys.* **427**, 147 (2004).
- ²⁷P. Lesaffre, J.-P. Chieze, and S. Cabrit, *Astron. Astrophys.* **427**, 157 (2004b).
- ²⁸D. Xu and D. Li, *Astrophys. J.* **833**, 90 (2016).
- ²⁹D. Xu, D. Li, N. Yue, and P. F. Goldsmith, *Astrophys. J.* **819**, 22 (2016).
- ³⁰P. F. Goldsmith, T. Velusamy, D. Li, and W. D. Langer, *Astrophys. J.* **715**, 1370 (2010).
- ³¹G. Cosentino, I. Jiménez-Serra, P. Caselli, J. D. Henshaw, A. T. Barnes, J. C. Tan, S. Viti, F. Fontani, and B. Wu, *Astrophys. J. Lett.* **881**, L42 (2019).
- ³²D. Schaeffer, W. Fox, J. Matteucci, K. Lezhnin, A. Bhattacharjee, and K. Germaschewski, *Phys. Plasmas* **27**, 042901 (2020).
- ³³M. Nakanotani, R. P. Camata, R. R. Arslanbekov, and G. P. Zank, *Phys. Rev. E* **105**, 045209 (2022).
- ³⁴D. R. Russell, G. C. Burdiak, J. J. Carroll-Nellenback, J. Halliday, J. Hare, S. Merlini, L. G. Suttle, V. Valenzuela-Villaseca, S. Eardley, J. A. Fullalove *et al.*, *Phys. Rev. Lett.* **129**, 225001 (2022).
- ³⁵D. Russell, G. Burdiak, J. Carroll-Nellenback, J. Halliday, J. Hare, S. Merlini, L. Suttle, V. Valenzuela-Villaseca, S. Eardley, J. Fullalove *et al.*, *J. Plasma Phys.* **89**, 915890401 (2023).
- ³⁶P. Mabey, B. Albertazzi, G. Rigon, J.-R. Marquès, C. Palmer, J. Topp-Muggleston, P. Perez-Martin, F. Kroll, F.-E. Brack, T. Cowan *et al.*, *Astrophys. J.* **896**, 167 (2020a).
- ³⁷L. I. Sedov, *J. Appl. Math. Mech.* **10**, 241 (1946).
- ³⁸G. Taylor, *Proc. R. Soc. London Ser. A. Math. Phys. Sci.* **201**, 175 (1950).
- ³⁹B. Albertazzi, J. Béard, A. Ciardi, T. Vinci, J. Albrecht, J. Billette, T. Burris-Mog, S. Chen, D. Da Silva, S. Dittrich *et al.*, *Rev. Sci. Instrum.* **84**, 043505 (2013).
- ⁴⁰I. H. Hutchinson, *Plasma Phys. Controlled Fusion* **44**, 2603 (2002).
- ⁴¹J. Miller, T. Boehly, A. Melchior, D. Meyerhofer, P. Celliers, J. Eggert, D. Hicks, C. Sorce, J. Oertel, and P. Emmel, *Rev. Sci. Instrum.* **78**, 034903 (2007).
- ⁴²J. MacFarlane, I. Golovkin, P. Wang, P. Woodruff, and N. Pereyra, *High Energy Density Phys.* **3**, 181 (2007).
- ⁴³J. Edmiston and C. Kennel, *J. Plasma Phys.* **32**, 429 (1984).
- ⁴⁴S. Braginskii, *Rev. Plasma Phys.* **1**, 205 (1965).
- ⁴⁵B. T. Draine, W. G. Roberge, and A. Dalgarno, *Astrophys. J., Part 1* **264**, 485 (1983).
- ⁴⁶D. Chernoff, D. Hollenbach, and C. F. McKee, *Astrophys. J.* **259**, L97 (1982).
- ⁴⁷I. B. Zeldovich, Y. P. Raizer, and W. D. Hayes, *Physics of Shock Waves and High-Temperature Hydrodynamic Phenomena* (Academic Press, New York, 1966), Vol. 1, pp. 489–515.
- ⁴⁸J. D. Sadler, H. Li, and K. A. Flippo, *Matter Radiat. Extremes* **6**, 065902 (2021).

- ⁴⁹M. Koenig, T. Michel, R. Yurchak, C. Michaut, B. Albertazzi, S. Laffite, E. Falize, L. Van Box Som, Y. Sakawa, T. Sano *et al.*, *Phys. Plasmas* **24**, 082707 (2017).
- ⁵⁰T. Michel, B. Albertazzi, P. Mabey, G. Rigon, F. Lefevre, L. V. B. Som, P. Barroso, S. Egashira, R. Kumar, C. Michaut *et al.*, *Astrophys. J.* **888**, 25 (2020).
- ⁵¹M. Edwards, A. MacKinnon, J. Zweiback, K. Shigemori, D. Ryutov, A. Rubenchik, K. Keilty, E. Liang, B. Remington, and T. Ditmire, *Phys. Rev. Lett.* **87**, 085004 (2001).
- ⁵²A. D. Edens, T. Ditmire, J. Hansen, M. Edwards, R. Adams, P. Rambo, L. Ruggles, I. Smith, and J. Porter, *Phys. Plasmas* **11**, 4968 (2004).
- ⁵³P. Mabey, T. Michel, B. Albertazzi, E. Falize, N. Charpentier, and M. Koenig, *Phys. Plasmas* **27**, 083302 (2020b).
- ⁵⁴A. Rigby, F. Cruz, B. Albertazzi, R. Bamford, A. R. Bell, J. E. Cross, F. Fraschetti, P. Graham, Y. Hara, P. Kozlowski *et al.*, *Nat. Phys.* **14**, 475 (2018).
- ⁵⁵J. D. Huba and S. Ossakow, *J. Atmos. Terr. Phys.* **43**, 775 (1981).
- ⁵⁶A. Triantafyllidis, J.-R. Marquès, S. Ferri, A. Calisti, Y. Benkadoum, Y. De León, A. Dearling, A. Ciardi, J. Béard, J.-M. Lagarrigue, N. Ozaki, M. Koenig, and B. Albertazzi, “Zeeman splitting observations in laser-produced magnetized blast waves,” *Matter Rad. Extremes* (submitted) (2025).
- ⁵⁷J. Derouillat, A. Beck, F. Pérez, T. Vinci, M. Chiamello, A. Grassi, M. Flé, G. Bouchard, I. Plotnikov, N. Aunai *et al.*, *Comput. Phys. Commun.* **222**, 351 (2018).
- ⁵⁸B. Fryxell, K. Olson, P. Ricker, F. X. Timmes, M. Zingale, D. Lamb, P. MacNeice, R. Rosner, J. Truran, and H. Tufo, *Astrophys. J. Suppl. Ser.* **131**, 273 (2000).
- ⁵⁹N. Aunai, R. Smets, A. Ciardi, P. Deegan, A. Jeandet, T. Payet, N. Guyot, and L. Darrieumerlou, *Comput. Phys. Commun.* **295**, 108966 (2024).
- ⁶⁰G. García-Segura, N. Langer, M. Rożyczka, and J. Franco, *Astrophys. J.* **517**, 767 (1999).
- ⁶¹A. Gintrand and Q. Moreno-Gelos, *Mon. Not. R Astron. Soc.* **520**, 1950 (2023).